Regulation of Cellular Heterogeneity and Rates of Symmetric and Asymmetric Divisions in Triple-Negative Breast Cancer

Citation: Granit, Roy Z., Hadas Masury, Reba Condiotti, Yaakov Fixler, Yael Gabai, Tzofia Glikman, Simona Dalin, et al. "Regulation of Cellular Heterogeneity and Rates of Symmetric and Asymmetric Divisions in Triple-Negative Breast Cancer." Cell Reports 24, no. 12 (September 2018): 3237–3250.

As Published: http://dx.doi.org/10.1016/j.celrep.2018.08.053

Publisher: Elsevier

Persistent URL: http://hdl.handle.net/1721.1/118749

Version: Final published version: final published article, as it appeared in a journal, conference proceedings, or other formally published context

Article

Cell Reports

Regulation of Cellular Heterogeneity and Rates of Symmetric and Asymmetric Divisions in Triple-Negative Breast Cancer

Graphical Abstract

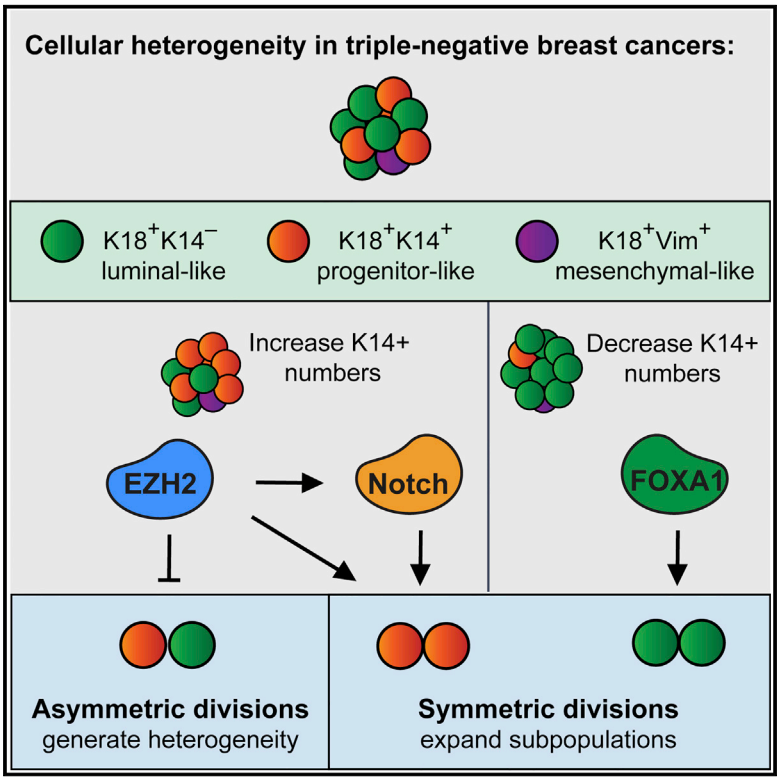

Highlights

- Triple-negative breast cancers display phenotypic cellular heterogeneity
- Asymmetric divisions that produce $K14^+$ and $K14^-$ daughter cells generate heterogeneity
- $K14^+$ cancer cells display a progenitor-associated tumorigenic phenotype
- EZH2, Notch, KLF5, and NFIB increase $K14^+$ cell numbers and FOXA1 decreases them

Authors

Roy Z. Granit, Hadas Masury, Reba Condiotti, ..., Aviv Regev, David E. Root, Ittai Ben-Porath

Correspondence

ittaibp@mail.huji.ac.il

In Brief

Granit et al. study the sources of phenotypic cellular heterogeneity in triple-negative breast cancers. They find that cancer cells can undergo asymmetric divisions that produce $K14^+$ and $K14^-$ daughters and thereby generate heterogeneity. $K14^+$ cells possess a progenitor-associated, tumorigenic phenotype, and the authors identify regulators that control their relative numbers.

Data and Software Availability

GSE84149

Granit et al., 2018, Cell Reports *24*, 3237–3250
September 18, 2018
https://doi.org/10.1016/j.celrep.2018.08.053

CellPress

Cell Reports
Article

Regulation of Cellular Heterogeneity and Rates of Symmetric and Asymmetric Divisions in Triple-Negative Breast Cancer

Roy Z. Granit,[1,10] Hadas Masury,[1,10] Reba Condiotti,[1,10] Yaakov Fixler,[1] Yael Gabai,[1] Tzofia Glikman,[1] Simona Dalin,[1] Eitan Winter,[2] Yuval Nevo,[2] Einat Carmon,[3] Tamar Sella,[4] Amir Sonnenblick,[5] Tamar Peretz,[5] Ulrich Lehmann,[6] Keren Paz,[7] Federica Piccioni,[8] Aviv Regev,[8,9] David E. Root,[8] and Ittai Ben-Porath[1,11,*]

[1]Department of Developmental Biology and Cancer Research, Institute for Medical Research–Israel-Canada, The Hebrew University–Hadassah Medical School, Jerusalem 91120, Israel
[2]Info-CORE, Bioinformatics Unit of the I-CORE Computation Center at The Hebrew University and Hadassah, Jerusalem 91120, Israel
[3]Department of Surgery, Hadassah–Hebrew University Medical Center, Jerusalem 91120, Israel
[4]Department of Radiology, Hadassah–Hebrew University Medical Center, Jerusalem 91120, Israel
[5]Sharett Institute of Oncology, Hadassah–Hebrew University Medical Center, Jerusalem 91120, Israel
[6]Institute of Pathology, Medizinische Hochschule Hannover, 30625 Hannover, Germany
[7]Champions Oncology, Inc., Baltimore, MD 21205, USA
[8]Broad Institute of MIT and Harvard, Cambridge, MA 02142, USA
[9]Howard Hughes Medical Institute and David H. Koch Institute of Integrative Cancer Biology, Department of Biology, Massachusetts Institute of Technology, Cambridge, MA 02142, USA
[10]These authors contributed equally
[11]Lead Contact
*Correspondence: ittaibp@mail.huji.ac.il
https://doi.org/10.1016/j.celrep.2018.08.053

SUMMARY

Differentiation events contribute to phenotypic cellular heterogeneity within tumors and influence disease progression and response to therapy. Here, we dissect mechanisms controlling intratumoral heterogeneity within triple-negative basal-like breast cancers. Tumor cells expressing the cytokeratin K14 possess a differentiation state that is associated with that of normal luminal progenitors, and K14-negative cells are in a state closer to that of mature luminal cells. We show that cells can transition between these states through asymmetric divisions, which produce one K14$^+$ and one K14$^-$ daughter cell, and that these asymmetric divisions contribute to the generation of cellular heterogeneity. We identified several regulators that control the proportion of K14$^+$ cells in the population. EZH2 and Notch increase the numbers of K14$^+$ cells and their rates of symmetric divisions, and FOXA1 has an opposing effect. Our findings demonstrate that asymmetric divisions generate differentiation transitions and heterogeneity, and identify pathways that control breast cancer cellular composition.

INTRODUCTION

Cellular heterogeneity is observed in many tumor types and represents a major hurdle for effective therapy (Marusyk et al., 2012; Meacham and Morrison, 2013). Transitions between differentiation states are thought to contribute to phenotypic intratumoral heterogeneity. In breast cancer, subpopulations of stem-like tumor cells possessing self-renewal and differentiation capacity have been identified (Brooks et al., 2015). Recent studies suggest that, rather than following a unidirectional differentiation hierarchy, cancer cells are able to transition between stem-like and differentiated identities and can also exist in intermediate states (Chaffer et al., 2013; Patel et al., 2014; Roesch et al., 2010). Cancer cell populations were shown in some cases to reach stable equilibria between phenotypically distinct subpopulations, suggesting the existence of dynamics and regulators that influence cellular composition (Quintana et al., 2010; Gupta et al., 2011).

Lineage programs active in the normal mammary epithelium contribute to breast cancer cell differentiation state (Visvader and Stingl, 2014; Prat and Perou, 2011; Granit et al., 2014). The mammary epithelium contains basal cells (also termed myoepithelial), some of which possess the potential to function as mammary stem cells (MaSCs), as well as luminal progenitors and mature luminal cells (Visvader and Stingl, 2014). These cell types possess distinct traits and appear to include further cell subclasses (Shehata et al., 2012; Tornillo and Smalley, 2015; Fu et al., 2017, Wang et al., 2017). Breast cancer subtypes reflect these normal differentiation states: luminal, estrogen receptor (ER)-positive tumors express a gene signature associated with mature luminal cells, whereas basal-like breast cancers (which are mostly included in the triple-negative pathological group) express the signature of luminal progenitor cells and likely originate from them (Lim et al., 2009; Keller et al., 2012; Molyneux et al., 2010).

Basal-like tumor cells may possess a high degree of plasticity, allowing them to transition between basal, progenitor, and luminal states. A hallmark of these triple-negative breast cancers (TNBCs) is that they contain cells expressing basal keratins, such

as K5 and K14, often together with luminal keratins such as K8 and K18 (Prat and Perou, 2011; Badve et al., 2011), consistent with such plasticity. Cells displaying a partially mesenchymal state, which have likely undergone a partial epithelial-to-mesenchymal transition (EMT), are also present in these tumors (Yu et al., 2013). This high level of heterogeneity and apparent plasticity likely contribute to the aggressive nature of TNBCs and to the difficulty in their treatment. However, a detailed delineation of the differentiation states of cell subpopulations within these tumors, and of the mechanisms driving transitions between them, is lacking.

Here, we study lineage-associated differentiation transitions within triple-negative basal-like tumors and their contribution to cellular heterogeneity. We show that the K14-expressing subpopulation displays enhanced tumorigenicity associated with increased expression of a luminal-progenitor gene signature, whereas K14-negative cells display a more mature luminal state. We show that tumor cells can transition between these states through asymmetric divisions that generate distinct daughter cells and that this contributes to the generation of heterogeneity. We identify regulators that control the proportions of $K14^+$ cancer cells and that modulate the relative rates of symmetric and asymmetric divisions.

RESULTS

Heterogeneity in Cellular Differentiation State within Basal-like Breast Cancers

We examined the degree of cellular heterogeneity in a collection of triple-negative, basal-like breast cancers (Table S1) by co-staining for the luminal cytokeratin K18, the basal cytokeratin K14, and the mesenchymal marker vimentin (VIM). As expected, basal-like tumors exhibited heterogeneous staining patterns, with cells, often in close proximity, displaying different levels of these markers and their combinations (Figures 1A and 1B). Most tumors contained a majority of cells that expressed the luminal marker K18 (>50% in 36 of 45 tumors; range 2.2%–100%; average 63.1%), as well as cells that co-expressed K18 and K14 ($K18^+K14^+$ cells; present in 38 of 45 tumors; range 0.3%–59% of cells; average 6.8%; Figures 1A and 1B). Vimentin expression was observed in most tumors as well (32 of 45; range 0.04%–57.5% Vim^+ cells; average 9.2%) and was most often associated with K18 expression (on average 50% of Vim^+ cells co-expressed $K18^+$, and 7.6% co-expressed K14). Similar heterogeneity was observed, to varying degrees, in several patient-derived xenografts (PDXs) of TNBCs (Figure S1A). We found that basal-like cell lines, specifically those maintaining epithelial identity (termed "basal A"), retain some of this cellular heterogeneity and harbor three prominent subpopulations: $K18^+$; $K18^+K14^+$; and $K18^+VIM^+$ cells (Figures 1C, 1D, and S1B).

We isolated and profiled the transcriptomes of these three subpopulations from two cell lines (HCC70 and MDA-MB-468) and assessed whether they differ in their expression of gene signatures of normal human mammary cell types (Lim et al., 2009; Shehata et al., 2012; Figures S1C and S1D; Table S2). $K18^+$ ($K14^-VIM^-$) cells showed the highest correlation of gene expression with the signature of mature luminal cells, whereas the $K18^+K14^+$ subpopulation exhibited the highest correlation with the luminal progenitor signature (Figures 1E, S1E, and S1F; Table S2). The $K18^+VIM^+$ subpopulation showed the highest correlation with an EMT signature (Taube et al., 2010) as well as with the basal (MaSC) signature, consistent with a partially mesenchymal state and its association with normal basal cells (Ye et al., 2015).

We also found that $K18^+K14^+$ cells isolated from a human triple-negative PDX expressed luminal progenitor signature genes at higher levels than $K18^+K14^-$ cells (Figure 1F). These analyses indicate that TNBC cells display distinct identities along the mesenchymal-epithelial and basal-luminal differentiation axes: $K18^+VIM^+$ cells are partially mesenchymal; $K18^+$ cells possess an identity closer to mature luminal cells; and $K18^+K14^+$ cells are in a state associated with that of luminal progenitors.

$K18^+K14^+$ Cells Possess Enhanced Tumorigenicity

We next compared the tumorigenic capacity of the $K18^+K14^+$ and $K18^+K14^-$ subpopulations. We found that $K18^+K14^+$ cell percentages were increased upon dissemination to the lungs, either spontaneously from MDA-MD-468-derived xenograft tumors or upon injection to the tail vein (Figures 2A, 2B, and S2A). The $K14^+$ state may therefore be advantageous for metastatic seeding, consistent with previous work (Cheung et al., 2013). As we could not isolate live cells based on $K18^+K14^+$ expression due to the necessity of cell fixation for keratin staining, we used a previously described reporter construct, in which GFP is driven by the K14 promoter (Granit et al., 2013; Figure S2B). GFP^{high} cells isolated from HCC70 and HCC1937 lines infected with this reporter were enriched for $K14^+$ cells relative to the GFP^- population by 1.5- to 2.5-fold, with no change in K18, which is expressed in nearly all cells (Figures S2C–S2G). The GFP^{high} cells showed enhanced tumor formation and tumor growth rates relative to GFP^- cells (Figures 2C–2E), supporting the notion that the $K18^+K14^+$ subpopulation possesses enhanced tumorigenicity.

Basal-like Breast Cancer Cells Undergo Asymmetric Divisions

We next asked whether transitions of tumor cells between differentiation states could be directly detected. Asymmetric cell divisions, in which the two daughter cells differ in phenotype from one another, provide a mechanism for differentiation transitions (Morrison and Kimble, 2006). To test whether asymmetric divisions occur in basal-like breast cancer cell populations, we conducted a bromodeoxyuridine (BrdU) pulse-chase assay: we treated sparsely seeded HCC70 cells with BrdU to label cells in S phase, waited 18–24 hr to allow generation of BrdU-labeled mitotic cell doublets, and then fixed and stained the cells for BrdU, K14, and K18 (Figure 3A). Pairs of $BrdU^+$ cells that were closely positioned in isolation from other cells and showed identical BrdU staining patterns were scored as mitotic products (Figure 3B). As expected, such doublets were rare when cells were fixed immediately after BrdU treatment (Figure S3A). We found that the majority of HCC70 cell divisions were symmetric, producing daughter cells that were either both $K14^-$ or both $K14^+$ (all co-expressing K18); however, ~9% of cell divisions were asymmetric, giving rise to one $K14^-$ and one $K14^+$ daughter cell (Figures 3B and 3C). Other basal-like lines showed a similar distribution of division types, with somewhat lower rates of

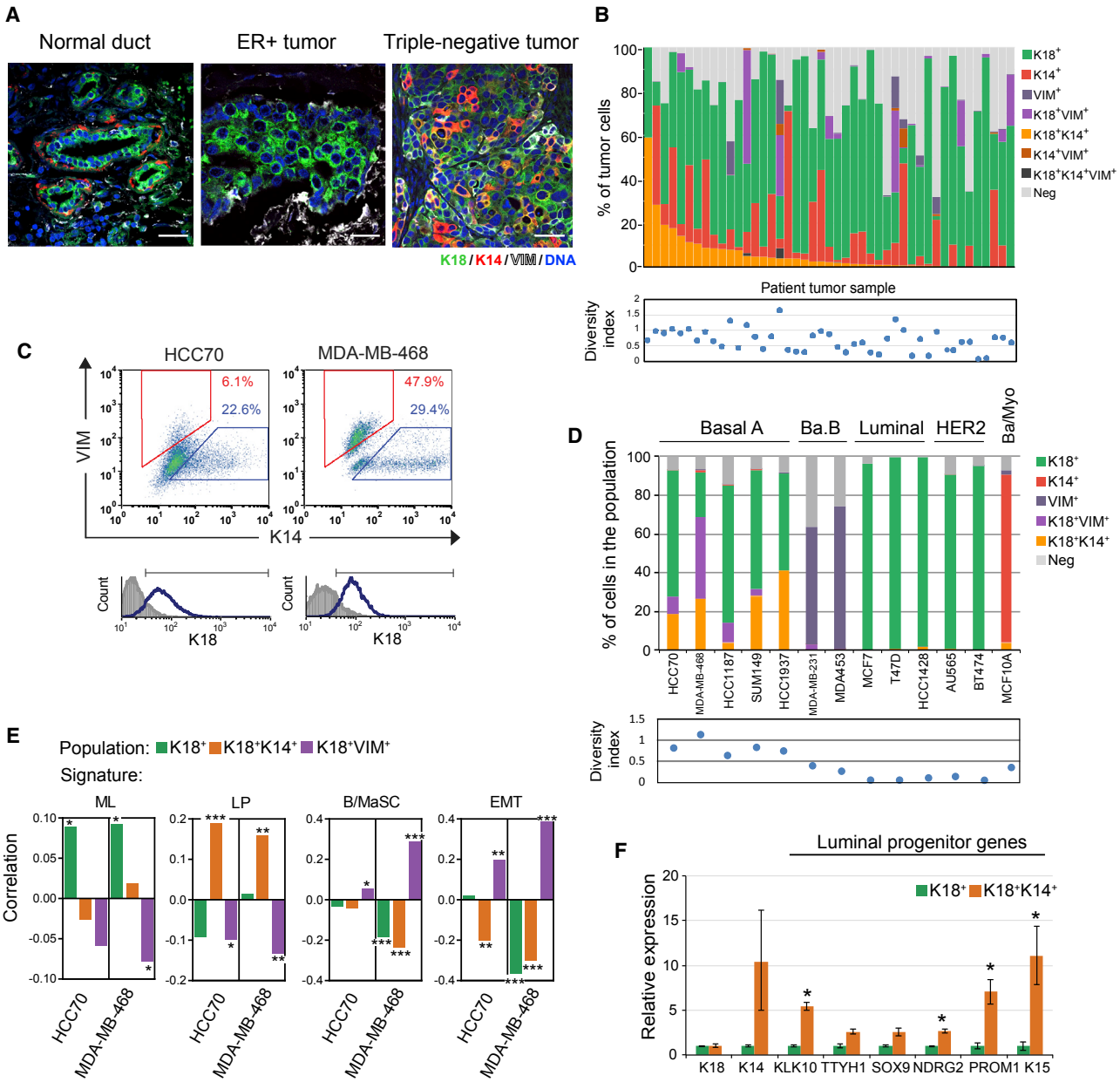

Figure 1. Basal-like Breast Cancers Harbor Cell Subpopulations with Distinct Differentiation States

(A) Co-staining of K18 (green), K14 (red), and vimentin (white) in sections of normal human breast, an ER+ luminal breast tumor, and a triple-negative tumor. Double-positive $K18^+K14^+$ cells appear as yellow or orange. The scale bars represent 50 μm.

(B) Percentages of cells stained positive for K18, K14, and vimentin and their combinations in a panel of 45 TNBCs. Lower panel shows the intratumoral Shannon diversity index values.

(C) FACS analysis of K18, K14, and vimentin expression in representative basal-like cell lines. Gates indicate $K18^+K14^+$ cells (blue) and $K18^+VIM^+$ cells (red). K18 staining histograms for each cell line are shown in lower panels, with marker indicating $K18^+$ range.

(D) Percentages of cell subpopulations in cell lines representing different breast cancer subtypes, as analyzed by FACS. Lower panel shows diversity index. Ba.B, basal B; Ba/Myo, immortalized basal (myoepithelial); HER2, HER2 overexpressing.

(E) Correlation values of the expression profiles of the $K18^+$, $K18^+K14^+$, and $K18^+VIM^+$ subpopulations isolated from HCC70 and MDA-MB-468 cells, with the indicated lineage-associated gene signatures. Positive correlations indicate preferential expression of signature genes in the tested cell population relative to other subpopulations and vice versa. B/MaSC, basal/mammary stem cell; EMT, epithelial mesenchymal transition; LP, luminal progenitor; ML, mature luminal. $^*p < 0.05$, $^{**}p < 0.005$, and $^{***}p < 0.0005$ of Spearman correlation.

(F) qRT-PCR analysis of genes representing the luminal progenitor signature in $K18^+$ and $K18^+K14^+$ cell populations isolated from a patient-derived xenograft of a TNBC (PDX1017). Values indicate mean of n = 3 replicates ± SEM. $^*p < 0.05$; Student's t test.

See also Figure S1 and Tables S1 and S2.

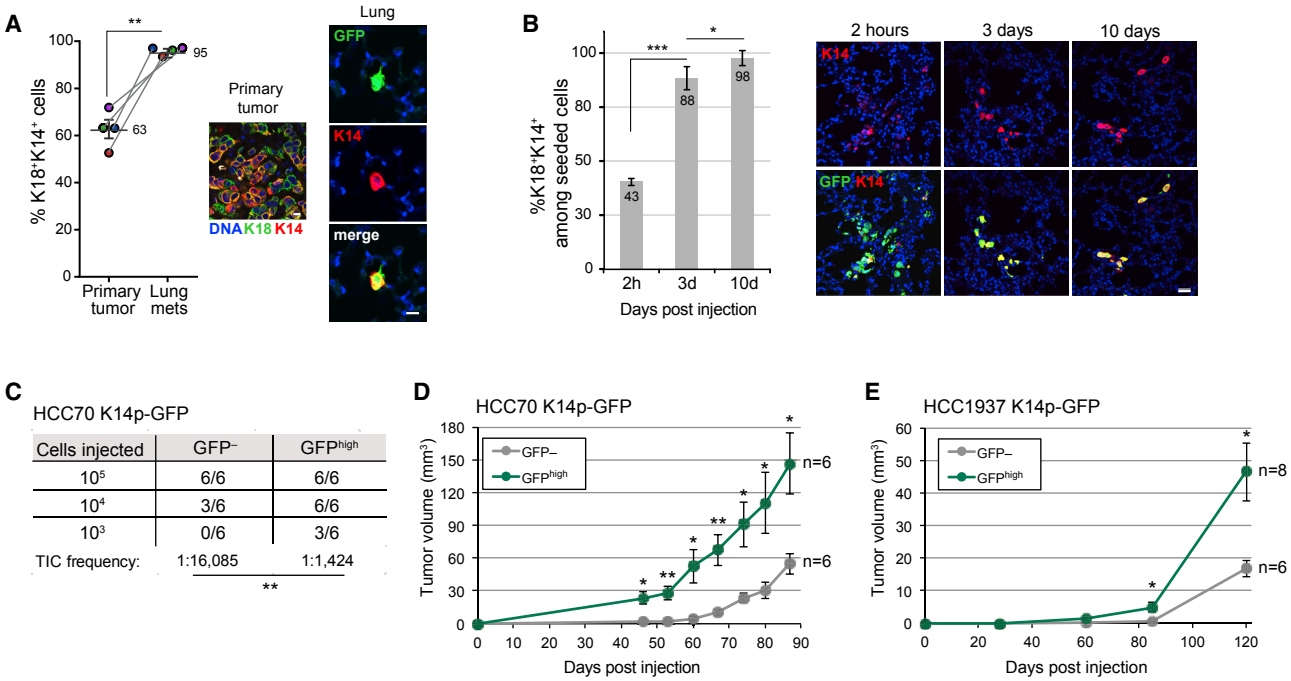

Figure 2. Increased Tumorigenicity of K18$^+$K14$^+$ Cells

(A) Percentage of K18$^+$K14$^+$ cells in primary GFP-labeled MDA-MB-468 xenograft tumors and in lung metastases originating from these tumors. Lines connect values of tumors and lungs from the same mouse; n = 4 mice. Images show a tumor section and a metastatic cell in a lung section stained with indicated antibodies. The scale bars represent 10 μm.

(B) Quantification (left) and images (right) of the percentage of K18$^+$K14$^+$ cells in lung metastases seeded by MDA-MB-468 cells injected into mouse tail veins at the indicated times. n = 3 mice in each point. The scale bar represents 25 μm.

(C) Numbers of tumors formed by GFP$^-$ and GFP^{high} subpopulations sorted from HCC70 cells expressing a K14-promoter-driven GFP reporter (K14p-GFP) after injection into NOD-SCID mouse mammary glands in limiting dilutions. (Left) Injected cell numbers are shown; values indicate tumors formed out of n = 6 mammary glands injected; (bottom) calculated tumor-initiating cell (TIC) frequency in each subpopulation is shown. **p < 0.005 by ELDA.

(D) Growth curves of tumors formed by 10^5 GFP$^-$ and GFP^{high} cells, sorted from HCC70 cells infected with the K14p-GFP reporter, and injected into mammary glands of NOD-SCID mice. n = 6 tumors per group.

(E) Growth curves of tumors formed by 2×10^3 GFP$^-$ and GFP^{high} cells, sorted from HCC1937 cells infected with the K14p-GFP reporter, and injected into mammary glands of NSG mice. n = 8 and n = 6 tumors for GFP$^-$ and GFP^{high} cells, respectively.

All values indicate mean ± SEM. *p < 0.05; **p < 0.005; ***p < 0.0005; t test. See also Figure S2.

asymmetric divisions (Figures 3C and 3D). Genomic sequencing of K18$^+$K14$^-$ and K18$^+$K14$^+$ HCC70 cell subpopulations did not reveal any copy number variations or changes in DNA methylation in the *KRT14* gene (Figures S3B and S3C), indicating that the observed plasticity in K14 staining is independent of these genomic alterations.

To further establish the asymmetric nature of the observed divisions, we tested the distribution of additional differentiation markers together with K14. We found that ALDH1A1, a known marker of stem and progenitor cells (Ginestier et al., 2007), was asymmetrically expressed in 9 of 16 divisions in which K14 was asymmetrically distributed but in none of 240 symmetric divisions ($p < 10^{-10}$ hypergeometric test), and in all cases, it was the K14$^+$ daughter cell that also expressed ALDH1A1 (Figure 3E).

We next tested whether asymmetric divisions occur within patient-derived tumors. We injected BrdU into mice carrying a PDX from a triple-negative breast cancer that contained K18$^+$ and K18$^+$K14$^+$ cells (PDX06; Figure S1A) and sacrificed them the following day. To detect mitotic cell pairs, tumor sections were stained for BrdU, K18, and K14. This revealed the presence of both symmetric and asymmetric divisions in the tumor, with asymmetric divisions that produced one K14$^+$ and one K14$^-$ cell (co-expressing K18) representing 10.6% of divisions (Figures 3F and 3G). Very few BrdU$^+$ cell doublets were found in mice sacrificed on the day of BrdU treatment (Figure S3D). These findings indicate that asymmetric divisions occur within basal-like breast cancer cell populations, generating K14-expressing and non-expressing cells.

Transitions in K14 Expression Generate Heterogeneity

To test the role of transitions between the K14$^+$ and K14$^-$ states in generating heterogeneity, we studied tumorspheres formed by HCC70 cells. If all divisions were symmetric and no transitions occurred, monoclonal tumorspheres would all be homogeneous, containing only K14$^-$ or K14$^+$ cells. However, every asymmetric division would generate a heterogeneous sphere containing both cell types. Thus, the occurrence of asymmetric divisions would be expected to produce an increasing percentage of heterogeneous spheres.

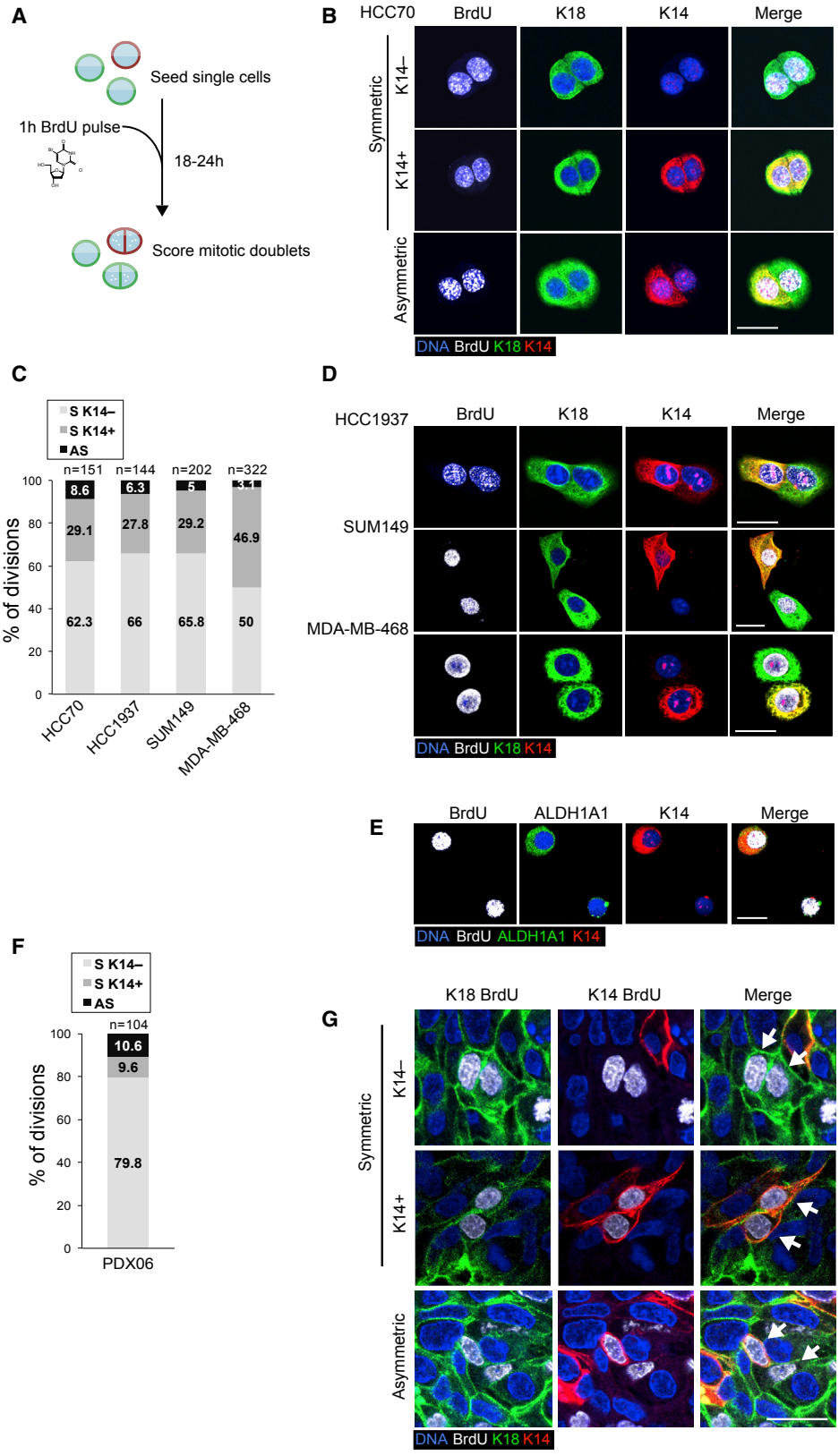

(legend on next page)

We tracked the numbers of $K14^+$ and $K14^-$ cells in growing tumorspheres over several days, after verifying that the great majority (~95%) of spheres were indeed of monoclonal origin (Figure S3E). The percentage of heterogeneous spheres, containing both $K14^+$ and $K14^-$ cells, rose as the spheres grew, from 29.5% of 4-cell spheres to 55% and 72% of spheres containing 6 and 8 cells, respectively (Figures 4A and 4B). Heterogeneous spheres showed a variety of ratios between $K14^+$ and $K14^-$ cells, excluding the possibility that individual single divergent cells transiently appeared within the spheres (Figure S3F). These findings indicate that cells indeed transition from one identity to another, giving rise to the observed heterogeneity. The percentages of homogeneous $K14^-$ and $K14^+$ spheres decreased with growth, suggesting that both $K14^+$ and $K14^-$ cells are able to undergo transitions.

To assess the contribution of asymmetric divisions to transitions, we treated tumorspheres with BrdU one day prior to fixation and stained them for K14 and BrdU to detect mitotic doublets. We detected asymmetric divisions producing one $K14^+$ and one $K14^-$ cell in approximately 20% of heterogeneous spheres scored (8 of 39; Figures 4C and 4D). Asymmetric divisions thus contribute to differentiation transitions within monoclonal cell populations.

EZH2 Maintains $K18^+K14^+$ Cell Numbers and Inhibits Asymmetric Divisions

We previously reported that short hairpin RNA (shRNA) silencing of EZH2, the catalytic subunit of the polycomb repressive complex 2 (PRC2), leads to reduced numbers of $K18^+K14^+$ cells (Granit et al., 2013). We tested the effects of treatment of HCC70 cells with the EZH2 inhibitor, GSK-126 (McCabe et al., 2012), and found that it similarly decreased the fraction of $K18^+K14^+$ cells in all tested basal-like cell lines (Figures 5A–5C). As expected, GSK-126 reduced global H3K27me3 levels, but it did not significantly affect cell viability (Figures S4A and S4B). EZH2 thus promotes the $K18^+K14^+$ state, consistent with its role in maintaining luminal progenitor identity in the normal breast (Michalak et al., 2013).

We next tested the influence of EZH2 inhibition on symmetric and asymmetric division rates. We found that the percentage of asymmetric divisions in cells following shRNA silencing of EZH2 was more than double that of control cells, whereas the percentage of symmetric $K14^+$ divisions was decreased (Figure 5D). Similar changes were observed in GSK-126-treated cells (Figure 5E). EZH2 silencing in HCC1937 cells also increased asymmetric division rates (Figure 5F). These results indicate that EZH2 acts to repress asymmetric divisions and promotes symmetric $K14^+$ divisions, a mechanism through which it could increase the numbers of $K18^+K14^+$ cells.

A Functional Screen Identifies Regulators of $K18^+K14^+$ Cell Numbers

To identify additional regulators that control the $K18^+K14^+$ cell fraction size, we conducted a functional screen, testing 177 candidate transcription factors and signaling proteins, based on subtype-specific expression and previously described roles in mammary cell differentiation (Table S3). We infected HCC70 cells seeded in 96-well plates with >500 shRNA-expressing viruses targeting these genes, as well as several control shRNAs, each in an individual well. Following selection for transduction, we quantified the percentage of $K14^+$ cells in each infected population by fluorescence-activated cell sorting (FACS) (Figures 6A, S5A, and S5B; Table S4). shRNA vectors targeting the gene encoding K14 itself, used as a positive control, showed the expected reduction in $K14^+$ cells (Figure S5A). Following a second screening step in which candidates were retested with multiple hairpins (Figure S5C), we identified four transcription factors whose silencing with multiple independent shRNAs consistently changed the fraction size of $K18^+K14^+$ cells in HCC70 cells (Figure 6B), and these showed similar effects also in HCC1937 cells (Figure 6C). Factors whose silencing led to reduced $K18^+K14^+$ fractions included KLF5, a regulator of embryonic stem cell identity, with a suggested oncogenic role in breast cancer (Jiang et al., 2008; Jia et al., 2016); NFIB, an oncogenic transcription factor that is often translocated in adenoid cystic breast carcinomas (Persson et al., 2009; Dooley et al., 2011); and RBPJ, the transcriptional mediator of Notch signaling (Koch et al., 2013). Silencing of FOXA1, a known regulator of mammary ductal growth that is highly expressed in luminal cells and luminal subtype tumors (Bernardo and Keri, 2012), had the opposite effect, increasing $K18^+K14^+$ cell numbers (Figures 6B and 6C).

To further verify their effects, we overexpressed these regulators in HCC70 cells. Overexpression of NFIB and KLF5 led to an increase in $K18^+K14^+$ cell numbers, and FOXA1 overexpression reduced these numbers, consistent with the converse consequences of their silencing (Figure 6D). RBPJ overexpression did not increase $K18^+K14^+$ cell numbers, likely due to the absence of enhanced upstream Notch signaling (Castel et al., 2013). mRNA sequencing (mRNA-seq) of cells in which each regulator was silenced indicated that the factors whose silencing reduced $K18^+K14^+$ cell numbers also reduced the expression of the luminal progenitor signature (Figures 6E and S5D; Table S5). NFIB, KLF5, and RBPJ-silenced cells also showed increased

Figure 3. Asymmetric Divisions Occur within Heterogeneous Cancer Cell Populations

(A) Procedure for identification of symmetric and asymmetric divisions: cells were sparsely seeded and treated with BrdU to label replicating cells and were fixed and stained 18–24 hr later to identify cell doublets representing mitotic products.

(B) HCC70 mitotic doublets stained for K18 (green), K14 (red), and BrdU (white). Images show a representative symmetric $K14^-$ division (top row), symmetric $K14^+$ division (middle row), and an asymmetric division in which one daughter cell is $K14^-$ and the other $K14^+$ (bottom row). All cells are $K18^+$.

(C) Distribution of symmetric (S) and asymmetric (AS) cell divisions in the indicated basal-like cell lines. n indicates the number of cell doublets scored.

(D) Representative images of asymmetric divisions of cells of indicated basal-like lines.

(E) HCC70 cell division showing asymmetric expression of K14 and of ALDH1A1.

(F) Symmetric and asymmetric division percentages scored in tumor sections of a TNBC patient-derived xenograft (PDX06), extracted one day after injection of BrdU to tumor-bearing mice, and stained for BrdU, K18, and K14. n indicates number of doublets scored. All cells scored co-express K18.

(G) Images of PDX sections scored in (F) showing symmetric (top two rows) and asymmetric divisions (bottom row).

The scale bars represent 25 μm. See also Figure S3.

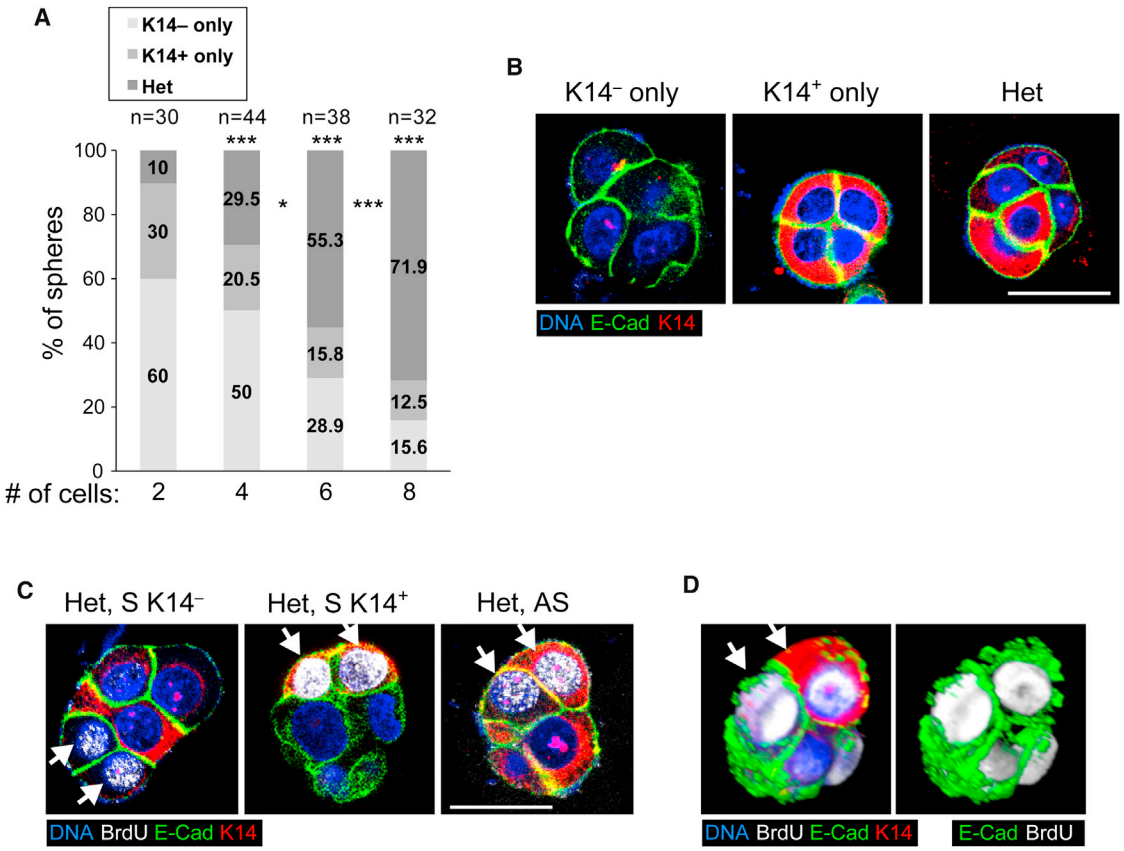

Figure 4. Asymmetric Divisions Contribute to Heterogeneity in Monoclonal Tumorspheres

(A) Percentages of HCC70 tumorspheres homogenously composed of $K18^+K14^-$ cells ($K14^-$ only), homogenously composed of $K18^+K14^+$ cells ($K14^+$ only), or containing both cell types (Het) at different tumorsphere sizes (# of cells). n indicates number of spheres analyzed. *$p < 0.05$; ***$p < 0.0005$; chi-square test, comparing the distributions to those observed at the two-cell stage (top asterisks) or between indicated sizes (asterisks between bars).

(B) Images of representative HCC70 tumorspheres after 4 days of growth, stained for K14 (red), E-cadherin for delineation of cell borders (green), and DNA (blue), showing homogeneous or heterogeneous cell composition.

(C) Examples of mitotic doublets (arrows) detected within heterogeneous tumorspheres (Het), stained for K14 (red), E-cadherin (green), BrdU (white), and DNA (blue). Symmetric $K14^-$ division (S $K14^-$, left panel), symmetric $K14^+$ division (S $K14^+$, middle panel), and asymmetric division (AS, right) are shown.

(D) 3D projection of an asymmetric division in a heterogeneous sphere. Right image shows same sphere with BrdU and E-cadherin channels only.

The scale bars represent 25 μm. See also Figure S3.

expression of the basal signature, suggesting that these factors promote luminal progenitor identity at the expense of basal identity.

Silencing of FOXA1 increased the expression of the luminal progenitor signature (Figure 6E). *FOXA1* mRNA levels are variable in basal-like breast cancers and are negatively correlated with *KRT14* and *EZH2* expression (Figures S6A and S6B). *FOXA1* expression was increased in EZH2-silenced cells (Figure S6C), consistent with these two regulators having opposing roles. We therefore tested the effects of FOXA1 silencing on symmetric and asymmetric division rates. Following FOXA1 silencing, cells displayed an increased number of symmetric $K14^+$ divisions, with reduced symmetric $K14^-$ divisions (Figures 6F and 6G), consistent with the observed increase in the numbers of $K18^+K14^+$ cells. FOXA1-silenced cells showed changes also in asymmetric division rates, but these were less substantial and inconsistent between lines (Figures 6F and 6G).

Together, these findings identify transcriptional regulators that control the composition of the tumor cell population and reveal FOXA1 as a negative regulator of $K18^+K14^+$ cell numbers and the balance between $K14^+$ and $K14^-$ symmetric divisions.

The Notch Pathway Regulates $K18^+K14^+$ Cell Numbers and Symmetric Division Rates

The functional screen revealed that silencing of RBPJ causes a substantial reduction in the numbers of $K18^+K14^+$ cells (Figures 6B and 6C), suggesting that the Notch pathway influences the composition of the cancer cell population. Expression of Notch transcriptional targets was reduced in RBPJ-silenced cells, indicating ongoing Notch activity (Figures 7A and 7B). Silencing of NOTCH1, or treatment with the γ-secretase inhibitor (GSI) LY-411575, had a similar effect on population composition, Notch target genes, and lineage genes (Figures 7C, 7D, and S7A–S7C). Conversely, NOTCH1 overexpression led to a dramatic

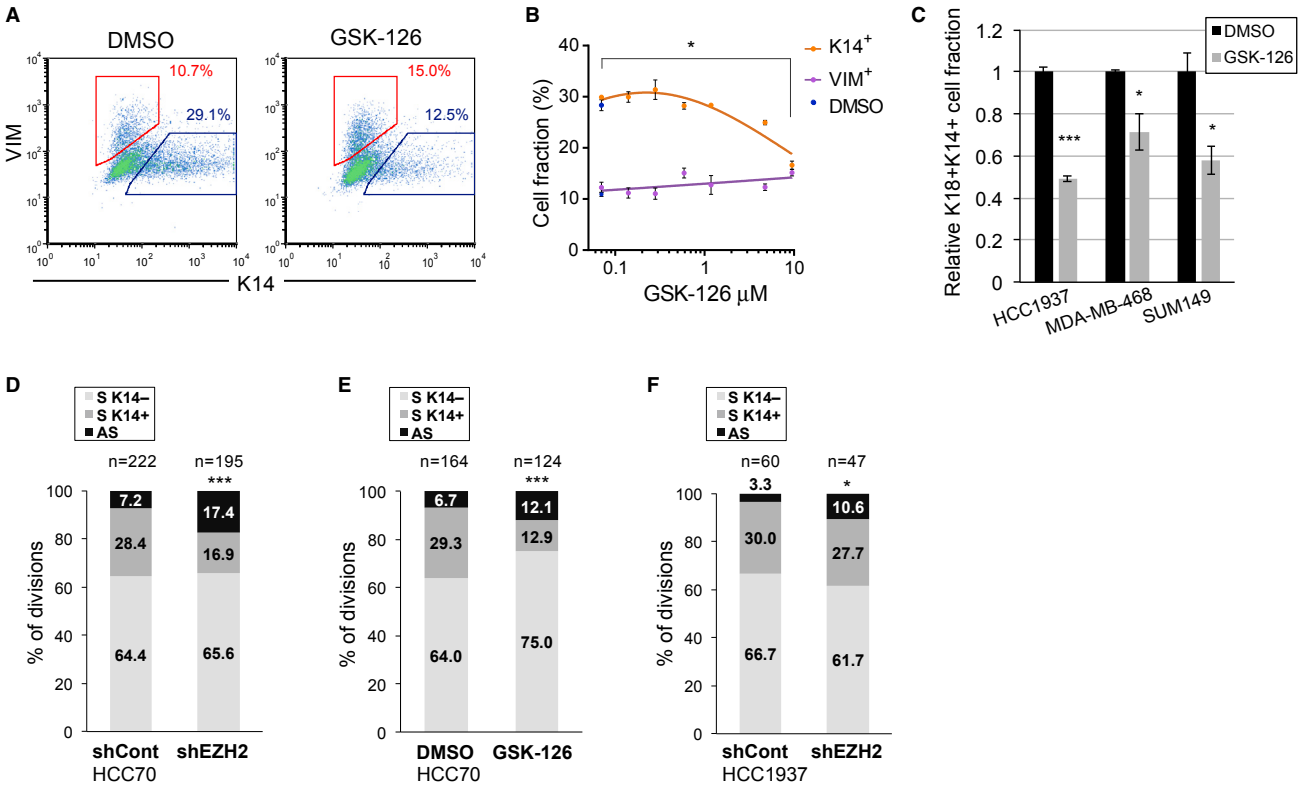

Figure 5. EZH2 Increases K18$^+$K14$^+$ Cell Numbers and Suppresses Asymmetric Divisions

(A) FACS analysis of HCC70 cells treated with the EZH2 inhibitor GSK-126 (10 μM, right) or with DMSO (left) for 3 days and stained for vimentin and K14. Gates indicate percentages of VIM$^+$ (red) and K14$^+$ (blue) cells.

(B) K14$^+$ and VIM$^+$ population percentages following treatment with indicated inhibitor concentrations for 3 days. Values indicate mean of n = 3 replicates ± SEM. *p < 0.05; t test.

(C) Relative fraction of K18$^+$K14$^+$ cells in indicated cell lines after treatment with GSK-126 for 3 days. Values are normalized to fraction in control cells; n = 3 replicates ± SEM.

(D) Distribution of S and AS divisions in HCC70 cells infected with shEZH2 or with a control shRNA (shCont) 6 days after infection.

(E) Distribution of cell division types in HCC70 cells after treatment with GSK-126 or DMSO for three days.

(F) Distribution of cell division types in HCC1937 cells infected with shEZH2 or shCont.

For (D)–(F), n indicates number of divisions scored. *p < 0.05; ***p < 0.0005; chi-square test. See also Figure S4 and Table S3.

increase in K18$^+$K14$^+$ numbers in both HCC70 and HCC1937 cells (Figures 7E, 7F, and S7D). Notch activity thus promotes the K18$^+$K14$^+$ identity. Interestingly, RBPJ silencing led also to a dramatic decrease in tumor formation by HCC70 cells (Figure S7E), highlighting a pro-tumorigenic function of this transcription factor.

Silencing of either NOTCH1 or RBPJ led to reduced numbers of symmetric K14$^+$ divisions and to increased numbers of symmetric K14$^-$ divisions (Figure 7G). Interestingly, unlike EZH2 inhibition, asymmetric division rates were also reduced. NOTCH1 overexpression exerted the opposite effect, increasing symmetric K14$^+$ divisions as well as asymmetric division rates (Figure 7H). Notch therefore appears to primarily promote symmetric K14$^+$ divisions at the expense of K14$^-$ symmetric divisions.

In light of their similar effects, we tested the regulatory relationship between EZH2 and Notch. We found that cells treated with the EZH2 inhibitor expressed reduced levels of Notch receptors and targets (Figure 7I). *EZH2* levels were, however, unchanged in GSI-treated or NOTCH1-silenced cells (Figure S7F), suggesting that EZH2 acts upstream to Notch in this context, consistent with previous work (Gonzalez et al., 2014). Indeed, treatment of RBPJ-silenced cells with GSK-126 did not further reduce K18$^+$K14$^+$ cell numbers (Figure 7J).

We also tested whether NFIB, which promotes K18$^+$K14$^+$ cell numbers, influences Notch. *NFIB* is expressed preferentially in basal-like breast cancers and in normal luminal progenitor and basal cells (Figures S7G and S7H). Cells silenced for NFIB expressed reduced levels of Notch receptors and targets, but not of *EZH2* (Figure 7K), suggesting that it acts upstream to Notch, independently of EZH2. Consistent with this, most genes deregulated in RBPJ-silenced cells were also deregulated by NFIB silencing (Figure S5D). GSI treatment led to a significant reduction in K18$^+$K14$^+$ cell numbers in NFIB-silenced cells, and GSK-126 had a more modest effect (Figure 7L). Together, these results suggest that Notch is a dominant regulator of K18$^+$K14$^+$ cell numbers and of asymmetric division rates and that it is positively regulated by both EZH2 and NFIB, whereas FOXA1 exerts an opposite effect (Figure 7M).

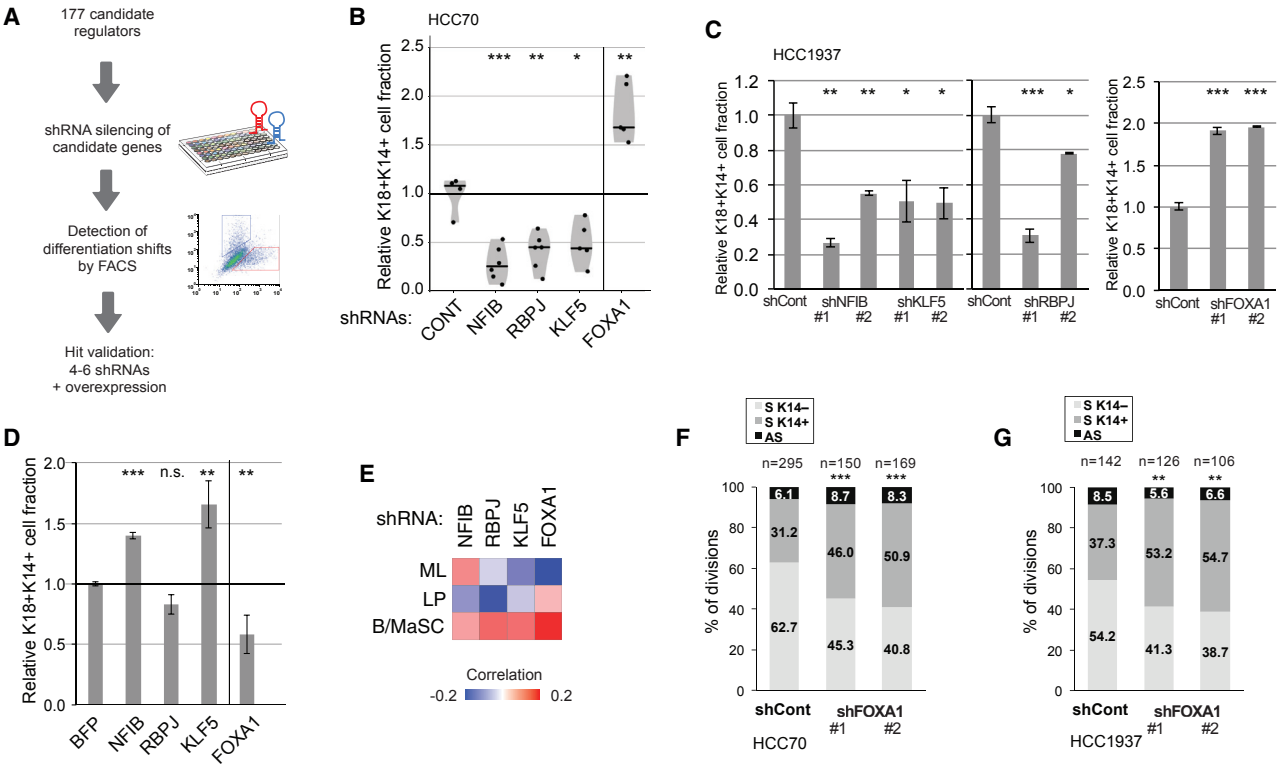

Figure 6. A Functional Screen Identifies Regulators of K18$^+$K14$^+$ Cell Numbers

(A) Screening procedure for identification of regulators of K18$^+$K14$^+$ cell fraction sizes. shRNAs against 177 candidate regulators and control shRNAs were introduced into HCC70 cells, and FACS analysis was conducted to assess changes in K18$^+$K14$^+$ cell percentages. Genes whose silencing increased or decreased K18$^+$K14$^+$ cell numbers were retested using additional shRNA vectors and by overexpression.

(B) K18$^+$K14$^+$ cell fractions in HCC70 cells silenced for the indicated regulators using 4–6 shRNAs, shown normalized to mean value of 4 different control vectors (CONT), as quantified by FACS. Dots indicate individual shRNAs; bars indicate median value for shRNAs targeting each gene. *p < 0.05; **p < 0.005; ***p < 0.0005; t test comparing values of tested shRNAs to the control vector values.

(C) K18$^+$K14$^+$ cell fractions in HCC1937 cells expressing two different shRNAs targeting the indicated genes, relative to cells expressing shCont, quantified by FACS. Values indicate mean of n = 3 replicates ± SEM. *p < 0.05, **p < 0.005, ***p < 0.0005, t test.

(D) K18$^+$K14$^+$ cell fractions in HCC70 cells overexpressing the indicated genes, shown relative to a blue fluorescent protein (BFP)-expressing control vector, quantified by FACS. Values are mean of replicates of three independent experiments ± SEM. **p < 0.005, ***p < 0.0005, t test.

(E) Correlations of gene expression profiles of cells silenced for each of the indicated regulators with normal mammary lineage gene signatures (indicated on left). Red and blue indicate positive and negative correlations, respectively. ML, mature luminal; LP, luminal progenitor, B/MaSC, basal/mammary stem cell.

(F) Distribution of cell division types of HCC70 cells expressing control (shCont) or two different FOXA1 shRNAs.

(G) Distribution of cell division types of HCC1937 cells expressing control (shCont) or two different FOXA1 shRNAs.

For (F) and (G): **p < 0.005; ***p < 0.0005 chi-square test. n indicates number of doublets scored. See also Figures S5 and S6 and Tables S3, S4, and S5.

DISCUSSION

Accumulating evidence indicates that non-genetic mechanisms substantially contribute to cellular heterogeneity within tumors and thereby to disease progression and resistance to therapy (Marusyk et al., 2012; Meacham and Morrison, 2013; Jordan et al., 2016; Roesch et al., 2010). The ability of cells to transition between differentiation states and adopt intermediate identities can generate a wide spectrum of cell phenotypes. Past analyses of basal-like breast tumor transcriptomes revealed the association of this subtype with luminal progenitor cells (Lim et al., 2009). However, the high level of cellular heterogeneity observed in these cancers suggests that they may often contain cells in a variety of differentiation states. We show here that some of these tumor cells possess an identity closer to that of luminal progenitors (manifested as a K18$^+$K14$^+$ profile), and others are in a state closer to mature luminal cells (exhibiting a K18$^+$K14$^-$ profile). As previously shown (Yu et al., 2013), some tumor cells adopt a distinct, partially mesenchymal state (manifested as a K18$^+$VIM$^+$ profile).

The association of the K18$^+$K14$^+$ profile with normal luminal progenitor identity is consistent with previous demonstrations of basal keratin expression in progenitor cells (Lim et al., 2009; Chakrabarti et al., 2012; Prat and Perou, 2011). Other markers used to identify luminal progenitors, such as CD49f, EpCAM, and ALDH1 (Visvader and Stingl, 2014; Smalley et al., 2012; Brooks et al., 2015), may allow for further enrichment of progenitor-like cells from these tumors. Recent studies suggest that several types of progenitors exist in the luminal compartment (Shehata et al., 2012; Tornillo and Smalley, 2015; Wang et al.,

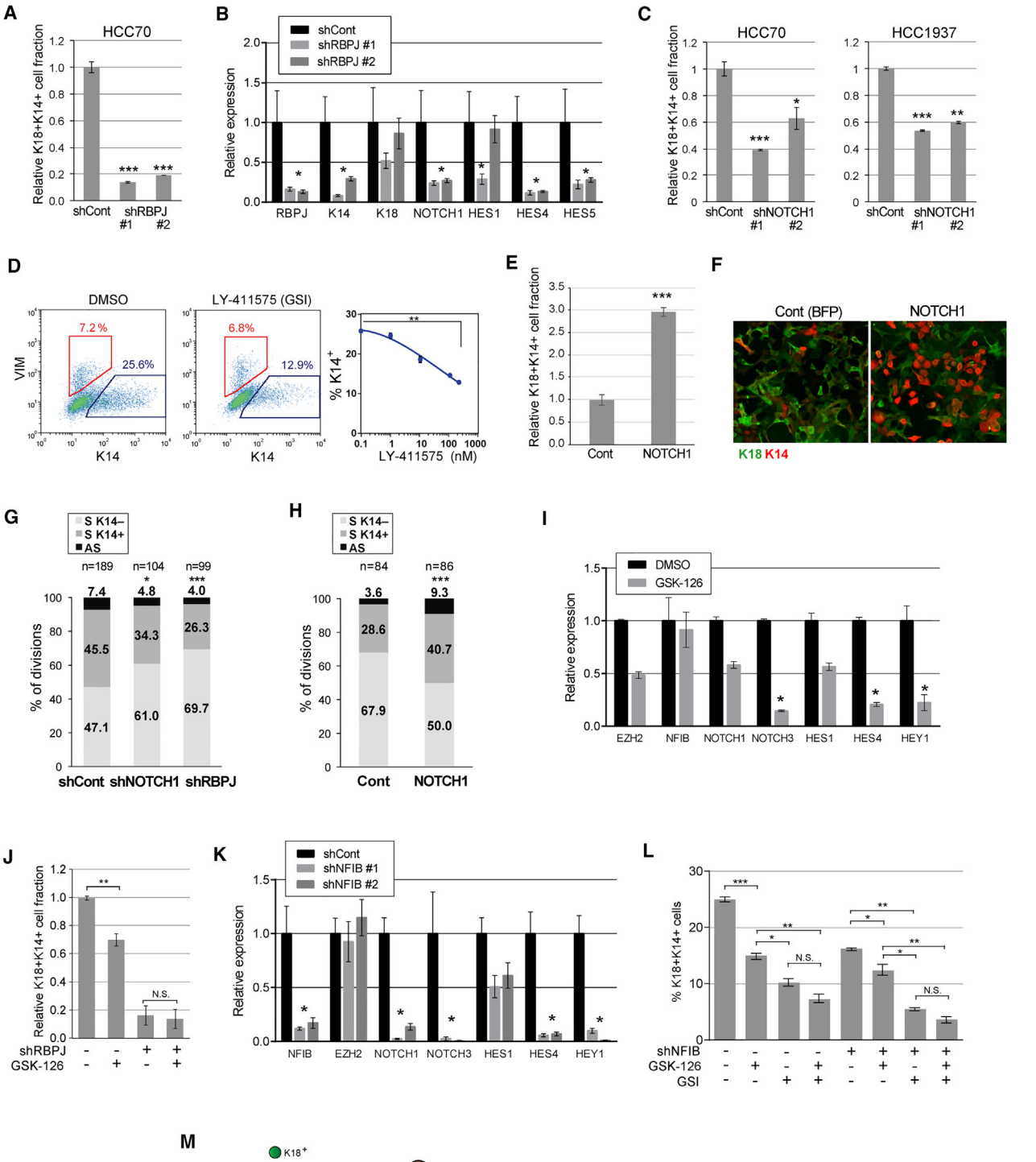

(legend on next page)

2017), and, therefore, different progenitor-like cell types may exist in tumors, with the $K18^+K14^+$ profile enriching for a particular subset. Co-expression of basal and luminal programs is observed in embryonic mammary precursors and in cell subsets of the postnatal prepubertal mouse gland (Pal et al., 2017; Wuidart et al., 2018); this suggests that the $K18^+K14^+$ breast cancer cells adopt a more primitive differentiation state.

Our finding that $K18^+K14^+$ cells possess increased tumorigenic capability are consistent with previous work showing that $K14^+$ cells are present in the invasive edges and metastases of breast cancers (Cheung et al., 2013) and with work showing increased expression of basal and progenitor markers in individually seeded metastatic cells (Lawson et al., 2015).

The processes allowing cancer cells to transition from one state to another are overall poorly characterized, and it is not clear whether such transitions are dependent on cell division. Asymmetric divisions represent one mechanism tying cell division to differentiation (Morrison and Kimble, 2006), and their occurrence has been shown in cell populations of several cancer types, including glioma, colon, and breast (Cicalese et al., 2009; Sugiarto et al., 2011; Bu et al., 2013). We directly show asymmetric divisions occurring within basal-like cell populations, producing one $K14^+$ and one $K14^-$ daughter cell. The detection of asymmetric divisions in a patient-derived xenograft provides indication that such divisions occur within tumors. Our finding that cellular heterogeneity progressively develops in growing monoclonal tumorspheres and that asymmetric divisions can be detected within them supports the notion that such divisions play a role in generating cellular heterogeneity through transitions between $K14^+$ and $K14^-$ states. We were not able to directly determine the identities of the mother cells of individual divisions due to the need for cell fixation to detect keratins. However, our findings suggest that both cell types are able to transition.

The ability to detect asymmetric divisions involving K14 may be related to the observation that cytokeratin filaments disintegrate during cytokinesis and are distributed between daughter cells prior to reassembly (Lane et al., 1982). Indeed, when cytokinesis was inhibited by blebbistatin, we could not detect cell pairs with asymmetric K14 distribution (data not shown). Asymmetric keratin distribution has also been observed in colon cancer cells (Bu et al., 2013).

We identify several regulators that control the percentage of $K14^+$ cells and thereby the composition of the tumor cell population: EZH2, Notch, KLF5 and NFIB act to increase the numbers of these cells, and their silencing leads to a new equilibrium in which the numbers of these cells are reduced. In contrast, FOXA1 and, as we have previously shown, GATA3 (Granit et al., 2013), perform the opposite function and are inhibited by EZH2. This is consistent with known roles of EZH2 and Notch in promoting luminal progenitor proliferation and function in the normal gland and the roles of FOXA1 and GATA3 in determining luminal identity (Michalak et al., 2013; Bouras et al., 2008; Bernardo and Keri, 2012). KLF5 and NFIB, although known to play other roles in breast cancer or in differentiation (Jiang et al., 2008; Jia et al., 2016; Persson et al., 2009; Dooley et al., 2011), were not previously linked with regulation of breast cancer cell identity. We show that EZH2, Notch, and FOXA1 influence the relative rates of symmetric and asymmetric divisions. The combined levels of activity of these regulators and others may thus determine the overall balance between division types, leading to a particular cellular composition.

Notch is known to regulate mammary differentiation and division symmetry in a variety of settings (Koch et al., 2013; Bouras et al., 2008; Harrison et al., 2010). We show that Notch is positively regulated by EZH2, consistent with previous work (Gonzalez et al., 2014), as well as by NFIB. Previous studies have implicated Notch and its target and negative regulator Numb in regulation of asymmetric divisions, and p53 and miR-34 have been linked to their activity (Bu et al., 2013; Tosoni et al., 2015). We could not detect asymmetric expression of Numb,

Figure 7. The Notch Pathway Regulates $K18^+K14^+$ Numbers and Symmetric Division Rates

(A) $K18^+K14^+$ cell fractions in HCC70 cells infected with two different shRNA vectors against RBPJ, relative to cells infected with shCont. Mean of n = 3 replicates ± SEM is shown.

(B) Relative expression of RBPJ and Notch targets measured by qRT-PCR in HCC70 cells infected with shCont or shRBPJ vectors. Mean of n = 3 replicates ± SEM is shown.

(C) $K18^+K14^+$ fractions in HCC70 and HCC1937 cells infected with two different shRNA vectors against NOTCH1, relative to cells expressing the shCont vector. Mean of n = 2 replicates ± SEM is shown.

(D) FACS analysis of HCC70 subpopulations after treatment for 3 days with the γ-secretase inhibitor (GSI) LY-411575 (200 nM) or DMSO (left), and quantification of $K18^+K14^+$ percentages following treatment with indicated inhibitor concentrations (right). Mean of n = 3 replicates ± SEM is shown.

(E) $K18^+K14^+$ cell fractions in HCC70 cells infected with a virus overexpressing NOTCH1 relative to cells expressing the control BFP gene. Mean of n = 4 replicates ± SEM is shown.

(F) Images of HCC70 cells expressing the control BFP vector or NOTCH1 and stained for K18 (green) and K14 (red).

(G) Distribution of cell division types of HCC70 cells silenced for NOTCH1 or RBPJ. n indicates cell doublets scored.

(H) Distribution of cell division types of HCC70 cells overexpressing NOTCH1 or a control (Luciferase) gene.

(I) Relative expression of EZH2, NFIB, and Notch receptors and target genes in HCC70 cells treated with GSK-126, measured by qRT-PCR.

(J) $K18^+K14^+$ fractions in HCC70 cells expressing shCont or shRBPJ, treated with GSI or DMSO. Means normalized to control of n = 3 independent experiments are shown.

(K) Relative expression of indicated genes in HCC70 cells infected with shCont or shNFIB vectors.

(L) $K18^+K14^+$ percentages in HCC70 cells expressing an shRNA against NFIB, and treated with GSK-126 for EZH2 inhibition, LY-411575 (GSI) for Notch inhibition, or with both inhibitors. Cells expressing shCont were used as controls for shNFIB cells. Mean of n = 3 replicates ± SEM is shown.

(M) Diagram illustrating the effects of indicated regulators on the composition of basal-like breast cancer cell populations. EZH2 and Notch increase $K18^+K14^+$ symmetric division rates and generate higher progenitor-like content, whereas FOXA1 restricts $K18^+K14^+$ symmetric divisions and reduces the numbers of these cells.

*p < 0.05; **p < 0.005; ***p < 0.0005. t test except (G) and (H) chi-square is shown. See also Figure S7 and Table S3.

but other related components of this network may influence Notch activity in the context described here.

Together, our findings shed light on the regulation of cellular heterogeneity and differentiation state in basal-like breast cancers and highlight several transcription factors that influence population composition. Manipulation of tumor composition can be achieved by pharmacologic means, including inhibitors of EZH2 and Notch, currently undergoing clinical evaluation. This supports the validity of approaches aimed at modulating cancer cell differentiation state, and thereby manipulating the cellular composition of tumors, as a component of treatment.

EXPERIMENTAL PROCEDURES

Human Tumor Samples and PDXs

Breast cancer sample sections were obtained from the Fox Chase Cancer Center (FCCC) Philadelphia, USA. PDX TNBC samples were obtained from Champions Oncology as part of Champions Personalized Oncology Service and grown as passages 3 and 4 (p3,4) in the mammary glands of immunocompromised female 4- to 6-week-old NSG (*NOD*; *Prkdc*^{scid}; *Il2rg*^{tm1Wjl}) mice, or from Hadassah Medical Center, grown and passaged in NSG-mice directly after surgical isolation. Patients whose samples were obtained through Champions signed an informed consent allowing the use of their tissue and its derived xenografts as well as their medical information for further research. Sample collection at Hadassah Medical Center was approved by the Institutional Review Board (Helsinki Committee) and was done under informed consent.

Cell Division Symmetry Assay and Tumorspheres

Cells were filtered twice through a 40-μm strainer and seeded sparsely on chambered cover slides (IBD-80826; Ibidi). 24 hr after seeding, the cells were treated for 2 hr with 10 μg/mL BrdU (Sigma-Aldrich) and 18–24 hr subsequently were fixed with cold ethanol and treated with 1M HCl. Residual acid was neutralized with 0.1M sodium tetraborate ($Na_2B_4O_7$) (pH = 8.5), and cells were stained for BrdU, K14, and K18 or ALDH1A1, using PBS + 10% fetal calf serum (FCS) for antibody suspension (2% FCS for washes), and with conjugated secondary antibodies. In experiments testing the effects of gene silencing, cells were seeded 4 days after infection with the appropriate shRNA lentivirus. Treatment of cells with Notch or EZH2 inhibitor was conducted for 3 days, starting one day before seeding. Stained cells were imaged and scored using a confocal microscope. Only cell doublets that showed identical BrdU stain pattern and were distant from other cells were scored. For detection of heterogeneity and asymmetric divisions in HCC70 tumorspheres, 6,000 cells were seeded after filtration in chambers coated with growth-factor-reduced Matrigel (cat no. 356230; Corning). Tumorspheres were grown for 3–6 days. Spheres were treated for 2 hr with 10 μg/mL BrdU one day prior to fixation and stained as above for BrdU, K14, and E-cadherin. For quantification of the percentage of polyclonal spheres, we seeded under this protocol a 1:1 mixture of HCC70 cells stably expressing GFP or mCherry and scored the percentage of spheres showing both colors, indicating polyclonality.

Tumor Transplantation and BrdU Labeling

For tumor-seeding experiments, HCC70 or HCC1937 cells infected with the K14p-GFP vector were sorted for GFP^{high} and GFP^{-} fractions by FACS, and cells were counted and injected in 10 μL culture medium containing 25% Matrigel (BD Biosciences) into no. 4 mammary glands of 6-week-old female non-obese diabetic (NOD)-severe combined immunodeficiency (SCID) (*NOD*; *Prkdc*^{scid}) or NSG mice as indicated. Tumors were measured externally by calipers and monitored for up to 5 months. Lack of tumor formation was validated by excision of the mammary gland. To evaluate the metastatic presence of K18^{+}K14^{+} cells, 1 × 10^{6} GFP-labeled MDA-MB-468 cells were suspended in 25% Matrigel in media, injected into no. 4 mammary glands of 6-week-old female NSG mice, and allowed to form tumors for 3 months. For lung-seeding experiments, 1 × 10^{6} GFP-labeled MDA-MB-468 cells were suspended in 100 μL F12 media and injected into the tail vein of NSG female mice. Primary tumors and lung sections were stained for K14, K18, and GFP. The percentage of K18^{+}K14^{+} cells among GFP^{+} cells was scored by image analysis using the CellProfiler software. For growth of patient-derived tumors, samples were minced and implanted into both no. 4 mammary glands of 6-week-old female NSG mice in 100 μL 50% Matrigel. Tumors were extracted 3–9 weeks after transplantation, minced, and suspended in media containing collagenase A (Roche; 1.5 mg/mL); incubated for 1 hr in a 37°C rocker; filtered through a 40-μM strainer; and stained and sorted to isolate K18^{+} and K18^{+}K14^{+} cell fractions. For BrdU labeling of PDXs, tumor-bearing NSG mice were injected after 3 months of tumor growth with BrdU (100 mg/kg in PBS) twice 3 hr apart and sacrificed one day later to allow detection of labeled mitotic doublets. Sections were stained for K18, K14, and BrdU, and doublets showing identical BrdU staining patterns and positioned in isolation from other BrdU^{+} cells were scored. Tumors used as negative controls for mitotic-doublet detection were excised two hours after BrdU treatment. The joint Institutional Animal Care and Use Committee of the Hebrew University and Hadassah Medical Center approved the study protocol for animal welfare. The Hebrew University is accredited by the Association for Assessment and Accreditation of Laboratory Animal Care International.

Cell Culture, Immune Staining and FACS, Functional Screening, and mRNA and DNA Sequencing

Please find detailed methods in Supplemental Information.

Statistical Methods

p values were mostly calculated using two-sided Student's t test as indicated. For comparisons of symmetric and asymmetric division distributions, a chi-square test was used. Significance of tumor-initiating experiments was done using extreme limiting dilution analysis (ELDA) (Hu and Smyth, 2009). The tumor diversity index was calculated using the Shannon-Wiener index $(H' = -\sum_{i=0}^{R} pi \times pi)$.

DATA AND SOFTWARE AVAILABILITY

The accession numbers for the expression datasets and whole-genome sequences of K14^{-} and K14^{+} HCC70 subpopulations reported in this paper are GEO: GSE84149 and SRA: SRP151223, respectively.

SUPPLEMENTAL INFORMATION

Supplemental Information includes Supplemental Experimental Procedures, seven figures, and five tables and can be found with this article online at https://doi.org/10.1016/j.celrep.2018.08.053.

ACKNOWLEDGMENTS

We thank Safa Hirbawi and Riham Smoom for assistance in virus preparation; Eleonora Medvedev for assistance in FACS analysis; Zakharia Menevitch for assistance in microscopy; Norma E. Kidess-Bassir for histological preparation; Jonathan P. Katz for the KLF5 expression vector; and Miriam Maoz, Michal Inbar, Aviad Zick, Ruth Shemer, Josh Moss, and Daniel Neiman for assistance in genomic sequencing and analysis. This study was supported by grants from the Israel Cancer Research Fund, the Israel Science Foundation (2309/15 and 2511/17), the United States-Israel Binational Science Foundation (2015205), the Israel Cancer Association, and the Jacob and Lena Joels Memorial Foundation (I.B.-P); the Lower Saxony-Israel Research Cooperation Program (I.B.-P. and U.L.); the Janey and Albert Sweet Scholarships, the Leonard and Faigel Shapiro Fellowship, and the Bester Scholarship Fund (R.Z.G.); and the Brody Foundation Fellowship (H.M.).

AUTHOR CONTRIBUTIONS

I.B.-P. designed the study and wrote the manuscript; R.Z.G., H.M., and R.C. designed and conducted the experiments; Y.F., Y.G., T.G., and S.D. assisted in experimentation and data analysis; E.W. and Y.N. conducted bioinformatic

analyses; E.C., T.S., A.S., T.P., U.L., and K.P. obtained and analyzed patient tumor samples; and F.P., A.R., and D.E.R. participated in functional screening and data analysis.

DECLARATION OF INTERESTS

K.P. is a shareholder at Champions Oncology. Other authors declare no competing interests.

Received: March 28, 2018
Revised: July 6, 2018
Accepted: August 17, 2018
Published: September 18, 2018

REFERENCES

Badve, S., Dabbs, D.J., Schnitt, S.J., Baehner, F.L., Decker, T., Eusebi, V., Fox, S.B., Ichihara, S., Jacquemier, J., Lakhani, S.R., et al. (2011). Basal-like and triple-negative breast cancers: a critical review with an emphasis on the implications for pathologists and oncologists. Mod. Pathol. *24*, 157–167.

Bernardo, G.M., and Keri, R.A. (2012). FOXA1: a transcription factor with parallel functions in development and cancer. Biosci. Rep. *32*, 113–130.

Bouras, T., Pal, B., Vaillant, F., Harburg, G., Asselin-Labat, M.L., Oakes, S.R., Lindeman, G.J., and Visvader, J.E. (2008). Notch signaling regulates mammary stem cell function and luminal cell-fate commitment. Cell Stem Cell *3*, 429–441.

Brooks, M.D., Burness, M.L., and Wicha, M.S. (2015). Therapeutic implications of cellular heterogeneity and plasticity in breast cancer. Cell Stem Cell *17*, 260–271.

Bu, P., Chen, K.Y., Chen, J.H., Wang, L., Walters, J., Shin, Y.J., Goerger, J.P., Sun, J., Witherspoon, M., Rakhilin, N., et al. (2013). A microRNA miR-34a-regulated bimodal switch targets Notch in colon cancer stem cells. Cell Stem Cell *12*, 602–615.

Castel, D., Mourikis, P., Bartels, S.J., Brinkman, A.B., Tajbakhsh, S., and Stunnenberg, H.G. (2013). Dynamic binding of RBPJ is determined by Notch signaling status. Genes Dev. *27*, 1059–1071.

Chaffer, C.L., Marjanovic, N.D., Lee, T., Bell, G., Kleer, C.G., Reinhardt, F., D'Alessio, A.C., Young, R.A., and Weinberg, R.A. (2013). Poised chromatin at the ZEB1 promoter enables breast cancer cell plasticity and enhances tumorigenicity. Cell *154*, 61–74.

Chakrabarti, R., Wei, Y., Romano, R.A., DeCoste, C., Kang, Y., and Sinha, S. (2012). Elf5 regulates mammary gland stem/progenitor cell fate by influencing notch signaling. Stem Cells *30*, 1496–1508.

Cheung, K.J., Gabrielson, E., Werb, Z., and Ewald, A.J. (2013). Collective invasion in breast cancer requires a conserved basal epithelial program. Cell *155*, 1639–1651.

Cicalese, A., Bonizzi, G., Pasi, C.E., Faretta, M., Ronzoni, S., Giulini, B., Brisken, C., Minucci, S., Di Fiore, P.P., and Pelicci, P.G. (2009). The tumor suppressor p53 regulates polarity of self-renewing divisions in mammary stem cells. Cell *138*, 1083–1095.

Dooley, A.L., Winslow, M.M., Chiang, D.Y., Banerji, S., Stransky, N., Dayton, T.L., Snyder, E.L., Senna, S., Whittaker, C.A., Bronson, R.T., et al. (2011). Nuclear factor I/B is an oncogene in small cell lung cancer. Genes Dev. *25*, 1470–1475.

Fu, N.Y., Rios, A.C., Pal, B., Law, C.W., Jamieson, P., Liu, R., Vaillant, F., Jackling, F., Liu, K.H., Smyth, G.K., et al. (2017). Identification of quiescent and spatially restricted mammary stem cells that are hormone responsive. Nat. Cell Biol. *19*, 164–176.

Ginestier, C., Hur, M.H., Charafe-Jauffret, E., Monville, F., Dutcher, J., Brown, M., Jacquemier, J., Viens, P., Kleer, C.G., Liu, S., et al. (2007). ALDH1 is a marker of normal and malignant human mammary stem cells and a predictor of poor clinical outcome. Cell Stem Cell *1*, 555–567.

Gonzalez, M.E., Moore, H.M., Li, X., Toy, K.A., Huang, W., Sabel, M.S., Kidwell, K.M., and Kleer, C.G. (2014). EZH2 expands breast stem cells through activation of NOTCH1 signaling. Proc. Natl. Acad. Sci. USA *111*, 3098–3103.

Granit, R.Z., Gabai, Y., Hadar, T., Karamansha, Y., Liberman, L., Waldhorn, I., Gat-Viks, I., Regev, A., Maly, B., Darash-Yahana, M., et al. (2013). EZH2 promotes a bi-lineage identity in basal-like breast cancer cells. Oncogene *32*, 3886–3895.

Granit, R.Z., Slyper, M., and Ben-Porath, I. (2014). Axes of differentiation in breast cancer: untangling stemness, lineage identity, and the epithelial to mesenchymal transition. Wiley Interdiscip. Rev. Syst. Biol. Med. *6*, 93–106.

Gupta, P.B., Fillmore, C.M., Jiang, G., Shapira, S.D., Tao, K., Kuperwasser, C., and Lander, E.S. (2011). Stochastic state transitions give rise to phenotypic equilibrium in populations of cancer cells. Cell *146*, 633–644.

Harrison, H., Farnie, G., Brennan, K.R., and Clarke, R.B. (2010). Breast cancer stem cells: something out of notching? Cancer Res. *70*, 8973–8976.

Hu, Y., and Smyth, G.K. (2009). ELDA: extreme limiting dilution analysis for comparing depleted and enriched populations in stem cell and other assays. J. Immunol. Methods *347*, 70–78.

Jia, L., Zhou, Z., Liang, H., Wu, J., Shi, P., Li, F., Wang, Z., Wang, C., Chen, W., Zhang, H., et al. (2016). KLF5 promotes breast cancer proliferation, migration and invasion in part by upregulating the transcription of TNFAIP2. Oncogene *35*, 2040–2051.

Jiang, J., Chan, Y.S., Loh, Y.H., Cai, J., Tong, G.Q., Lim, C.A., Robson, P., Zhong, S., and Ng, H.H. (2008). A core Klf circuitry regulates self-renewal of embryonic stem cells. Nat. Cell Biol. *10*, 353–360.

Jordan, N.V., Bardia, A., Wittner, B.S., Benes, C., Ligorio, M., Zheng, Y., Yu, M., Sundaresan, T.K., Licausi, J.A., Desai, R., et al. (2016). HER2 expression identifies dynamic functional states within circulating breast cancer cells. Nature *537*, 102–106.

Keller, P.J., Arendt, L.M., Skibinski, A., Logvinenko, T., Klebba, I., Dong, S., Smith, A.E., Prat, A., Perou, C.M., Gilmore, H., et al. (2012). Defining the cellular precursors to human breast cancer. Proc. Natl. Acad. Sci. USA *109*, 2772–2777.

Koch, U., Lehal, R., and Radtke, F. (2013). Stem cells living with a Notch. Development *140*, 689–704.

Lane, E.B., Goodman, S.L., and Trejdosiewicz, L.K. (1982). Disruption of the keratin filament network during epithelial cell division. EMBO J. *1*, 1365–1372.

Lawson, D.A., Bhakta, N.R., Kessenbrock, K., Prummel, K.D., Yu, Y., Takai, K., Zhou, A., Eyob, H., Balakrishnan, S., Wang, C.Y., et al. (2015). Single-cell analysis reveals a stem-cell program in human metastatic breast cancer cells. Nature *526*, 131–135.

Lim, E., Vaillant, F., Wu, D., Forrest, N.C., Pal, B., Hart, A.H., Asselin-Labat, M.L., Gyorki, D.E., Ward, T., Partanen, A., et al. (2009). Aberrant luminal progenitors as the candidate target population for basal tumor development in BRCA1 mutation carriers. Nat. Med. *15*, 907–913.

Marusyk, A., Almendro, V., and Polyak, K. (2012). Intra-tumour heterogeneity: a looking glass for cancer? Nat. Rev. Cancer *12*, 323–334.

McCabe, M.T., Ott, H.M., Ganji, G., Korenchuk, S., Thompson, C., Van Aller, G.S., Liu, Y., Graves, A.P., Della Pietra, A., 3rd, Diaz, E., et al. (2012). EZH2 inhibition as a therapeutic strategy for lymphoma with EZH2-activating mutations. Nature *492*, 108–112.

Meacham, C.E., and Morrison, S.J. (2013). Tumour heterogeneity and cancer cell plasticity. Nature *501*, 328–337.

Michalak, E.M., Nacerddine, K., Pietersen, A., Beuger, V., Pawlitzky, I., Cornelissen-Steijger, P., Wientjens, E., Tanger, E., Seibler, J., van Lohuizen, M., and Jonkers, J. (2013). Polycomb group gene Ezh2 regulates mammary gland morphogenesis and maintains the luminal progenitor pool. Stem Cells *31*, 1910–1920.

Molyneux, G., Geyer, F.C., Magnay, F.A., McCarthy, A., Kendrick, H., Natrajan, R., Mackay, A., Grigoriadis, A., Tutt, A., Ashworth, A., et al. (2010). BRCA1 basal-like breast cancers originate from luminal epithelial progenitors and not from basal stem cells. Cell Stem Cell *7*, 403–417.

Morrison, S.J., and Kimble, J. (2006). Asymmetric and symmetric stem-cell divisions in development and cancer. Nature *441*, 1068–1074.

Pal, B., Chen, Y., Vaillant, F., Jamieson, P., Gordon, L., Rios, A.C., Wilcox, S., Fu, N., Liu, K.H., Jackling, F.C., et al. (2017). Construction of developmental lineage relationships in the mouse mammary gland by single-cell RNA profiling. Nat. Commun. *8*, 1627.

Patel, A.P., Tirosh, I., Trombetta, J.J., Shalek, A.K., Gillespie, S.M., Wakimoto, H., Cahill, D.P., Nahed, B.V., Curry, W.T., Martuza, R.L., et al. (2014). Single-cell RNA-seq highlights intratumoral heterogeneity in primary glioblastoma. Science *344*, 1396–1401.

Persson, M., Andrén, Y., Mark, J., Horlings, H.M., Persson, F., and Stenman, G. (2009). Recurrent fusion of MYB and NFIB transcription factor genes in carcinomas of the breast and head and neck. Proc. Natl. Acad. Sci. USA *106*, 18740–18744.

Prat, A., and Perou, C.M. (2011). Deconstructing the molecular portraits of breast cancer. Mol. Oncol. *5*, 5–23.

Quintana, E., Shackleton, M., Foster, H.R., Fullen, D.R., Sabel, M.S., Johnson, T.M., and Morrison, S.J. (2010). Phenotypic heterogeneity among tumorigenic melanoma cells from patients that is reversible and not hierarchically organized. Cancer Cell *18*, 510–523.

Roesch, A., Fukunaga-Kalabis, M., Schmidt, E.C., Zabierowski, S.E., Brafford, P.A., Vultur, A., Basu, D., Gimotty, P., Vogt, T., and Herlyn, M. (2010). A temporarily distinct subpopulation of slow-cycling melanoma cells is required for continuous tumor growth. Cell *141*, 583–594.

Shehata, M., Teschendorff, A., Sharp, G., Novcic, N., Russell, I.A., Avril, S., Prater, M., Eirew, P., Caldas, C., Watson, C.J., and Stingl, J. (2012). Phenotypic and functional characterisation of the luminal cell hierarchy of the mammary gland. Breast Cancer Res. *14*, R134.

Smalley, M.J., Kendrick, H., Sheridan, J.M., Regan, J.L., Prater, M.D., Lindeman, G.J., Watson, C.J., Visvader, J.E., and Stingl, J. (2012). Isolation of mouse mammary epithelial subpopulations: a comparison of leading methods. J. Mammary Gland Biol. Neoplasia *17*, 91–97.

Sugiarto, S., Persson, A.I., Munoz, E.G., Waldhuber, M., Lamagna, C., Andor, N., Hanecker, P., Ayers-Ringler, J., Phillips, J., Siu, J., et al. (2011). Asymmetry-defective oligodendrocyte progenitors are glioma precursors. Cancer Cell *20*, 328–340.

Taube, J.H., Herschkowitz, J.I., Komurov, K., Zhou, A.Y., Gupta, S., Yang, J., Hartwell, K., Onder, T.T., Gupta, P.B., Evans, K.W., et al. (2010). Core epithelial-to-mesenchymal transition interactome gene-expression signature is associated with claudin-low and metaplastic breast cancer subtypes. Proc. Natl. Acad. Sci. USA *107*, 15449–15454.

Tornillo, G., and Smalley, M.J. (2015). ERrrr…where are the progenitors? Hormone receptors and mammary cell heterogeneity. J. Mammary Gland Biol. Neoplasia *20*, 63–73.

Tosoni, D., Zecchini, S., Coazzoli, M., Colaluca, I., Mazzarol, G., Rubio, A., Caccia, M., Villa, E., Zilian, O., Di Fiore, P.P., and Pece, S. (2015). The Numb/p53 circuitry couples replicative self-renewal and tumor suppression in mammary epithelial cells. J. Cell Biol. *211*, 845–862.

Visvader, J.E., and Stingl, J. (2014). Mammary stem cells and the differentiation hierarchy: current status and perspectives. Genes Dev. *28*, 1143–1158.

Wang, C., Christin, J.R., Oktay, M.H., and Guo, W. (2017). Lineage-biased stem cells maintain estrogen-receptor-positive and -negative mouse mammary luminal lineages. Cell Rep. *18*, 2825–2835.

Wuidart, A., Sifrim, A., Fioramonti, M., Matsumura, S., Brisebarre, A., Brown, D., Centonze, A., Dannau, A., Dubois, C., Van Keymeulen, A., et al. (2018). Early lineage segregation of multipotent embryonic mammary gland progenitors. Nat. Cell Biol. *20*, 666–676.

Ye, X., Tam, W.L., Shibue, T., Kaygusuz, Y., Reinhardt, F., Ng Eaton, E., and Weinberg, R.A. (2015). Distinct EMT programs control normal mammary stem cells and tumour-initiating cells. Nature *525*, 256–260.

Yu, M., Bardia, A., Wittner, B.S., Stott, S.L., Smas, M.E., Ting, D.T., Isakoff, S.J., Ciciliano, J.C., Wells, M.N., Shah, A.M., et al. (2013). Circulating breast tumor cells exhibit dynamic changes in epithelial and mesenchymal composition. Science *339*, 580–584.